THE JOURNAL OF PHYSICAL CHEMISTRY C

Article

pubs.acs.org/JPCC

Influence of the Anchoring Modes on the Electronic and Photovoltaic Properties of D−π−A Dyes

Masataka Katono, Takeru Bessho, Mateusz Wielopolski, Magdalena Marszalek, Jacques-E. Moser, Robin Humphry-Baker, Shaik M. Zakeeruddin,* and Michael Grätzel*

Laboratory for Photonics and Interfaces, Institute of Chemical Sciences and Engineering, Swiss Federal Institute of Technology, CH-1015 Lausanne, Switzerland

Supporting Information

ABSTRACT: Five new donor−π-bridge−acceptor (D−π−A) organic sensitizers with cyano and/or triple bond substituted benzoic acid as acceptor/anchoring groups were synthesized and tested for their performance in dye-sensitized solar cells (DSCs). The systematic incorporation of a cyano group on the benzoic acid anchoring part and an additional acetylene bond at the *para*-position to −COOH lead to a variation of the photoelectrochemical properties, electronic transitions, and device performances. Characterization of the molecular structure, the electronic/optical properties of the dyes, as well as their photovoltaic performance in DSCs was accomplished by means of electrochemistry, quantum chemical methods, and various spectroscopic techniques such as photoinduced absorption, steady-state spectroscopy, and time-resolved transient absorption studies on femto- and nanosecond time scales. Thereby, significant dependence of DSCs performances on the substituents and anchoring groups was observed. In general, cyano substituents lead to improved DSCs performances. On the other hand, the insertion of an acetylene linker in combination with a cyano group does not enhance the device efficiencies. Devices composed of a *para*-cyano benzoic acid as anchor revealed maximum IPCE values of 80% with a PCE of 4.50% at AM 1.5 G illumination (100 mW cm^{-2}) due to retarded charge recombination dynamics.

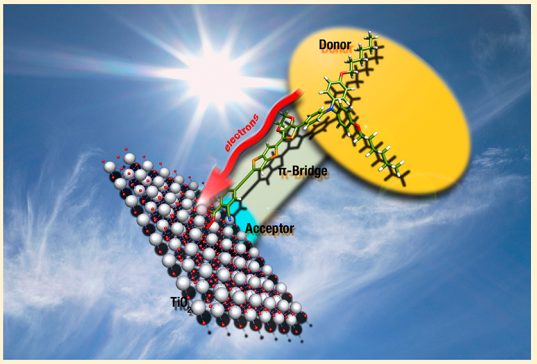

1. INTRODUCTION

Dye-sensitized solar cells (DSCs) have attracted high interest due to their remarkable performances in converting solar energy to electricity at relatively low cost as compared to conventional silicon-based photovoltaic devices.[1] One of the key roles in DSCs is attributed to the sensitizers, which are responsible for light absorption and the generation of electric charges. Among these, ruthenium sensitizers exhibit record solar to electricity power conversion efficiencies (PCEs) of 11−12% under AM 1.5 G irradiation.[2] A record PCE of 12.3% was achieved with a donor−π-bridge−acceptor zinc porphyrin in combination with a cobalt-based redox electrolyte.[2e] Recently, however, more and more research activities focus on the design and development of new metal-free organic sensitizers with the purpose of increasing the PCEs.[3,4] The high extinction coefficients of organic dyes and the ease of tuning their spectral properties by standard synthetic methods turned out to be highly advantageous. Most efficient photovoltaic performance was achieved when employing metal-free organic sensitizers of a donor−π-conjugated spacer−acceptor/anchoring (D−π−A) architecture. Lately, several synthetic strategies lead to the development of various donors based on coumarin, indoline, tetrahydroquinoline, triarylamine, heteroanthracene, and carbazole with a cyanoacrylic acid as the acceptor/anchoring unit. DSCs derived from these types of D−π−A systems have achieved up to 10% efficiency under AM 1.5 G full sunlight intensity.[3b] Even though many structural variations of the donor moieties have been reported, the acceptor/anchoring groups have been much less explored, notwithstanding the fact that they show a significant influence on the spectral response and device performance.

Recently, we have contributed to this field by reporting on the photovoltaic response of a D−π−A-type dye (coded as **KM-1**) containing cyanobenzoic acid as anchoring group.[5] To grasp the influence of the anchoring to TiO_2, herein we report the synthesis and application of new organic sensitizers with yet other anchoring moieties, that is, various substituted benzoic acids as acceptor/anchoring groups. In a further step, we investigate the substitution of the cyano and/or acetylene bond on the phenyl group to elucidate the impact on the optical properties and photovoltaic device performances. All structures of the new D−π−A sensitizers (coded as **KM-2**, **KM-3**, **KM-5**, and **KM-6**) are represented in Chart 1. The incorporation of benzoic acid was expected to extend the π-conjugation and promote a relatively planar structure of the whole molecule. Starting off with **KM-3** (no substituents on the benzoic acid) as

Received: May 9, 2012
Revised: July 23, 2012
Published: July 23, 2012

   dx.doi.org/10.1021/jp304490a | J. Phys. Chem. C 2012, 116, 16876−16884

Chart 1. Molecular Structures of KM Dyes

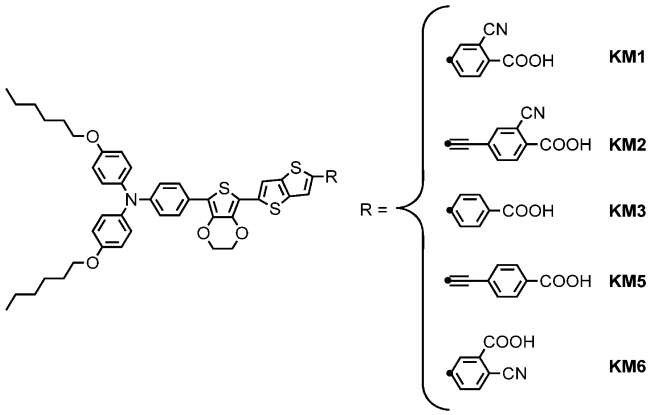

a reference, we systematically introduced a cyano group on the benzoic acid anchoring part in addition to an acetylene bond at the *para*-position to −COOH and studied the variations of the photoelectrochemical properties, electronic transitions, and device performances.

2. EXPERIMENTAL SECTION

2.1. Materials. All chemicals and solvents were purchased from commercial sources and used without further purification. For chromatographic purification, we used Silica Gel 60 (230−400 mesh, Merck, Germany). 4-(5-(7-(4-(Bis(4-(hexyloxy)-phenyl)amino)phenyl)-2,3-dihydrothieno[3,4-*b*][1,4]dioxin-5-yl)thieno[3,2-b]thiophen-2-yl)-2-cyanobenzoic acid (**KM-1**) was synthesized as reported earlier.[5]

2.2. Instruments. Absorption spectra (Cary 5, Varian), fluorescence spectra (Fluorolog 3, Horiba), and NMR spectra (AVANCE-400, Bruker) were used to characterize the dyes.

2.3. Syntheses of KM-2, KM-3, KM-5, and KM-6 Dyes. *Synthesis of Methyl 2-Cyano-4-(4,4,5,5-tetramethyl-1,3,2-dioxaborolan-2-yl)benzoate (**3**).* A 100 mL flask with a magnetic stirring bar, a septum inlet, and a condenser was charged with $Pd(dba)_2$ (0.17 g, 0.3 mmol) and tricyclohexylphosphine (0.20 g, 0.72 mmol) under nitrogen. Dioxane (35 mL) was added, and the resulting mixture was then stirred for 30 min at room temperature. Bis(pinacolato)diboron (2.79 g, 11 mmol), KOAc (1.47 g, 15 mmol), and **1** (1.96 g, 10 mmol) were added successively. After being stirred at 80 °C for 19 h, the reaction mixture was treated with water (30 mL). The product was extracted with toluene, washed with brine, and dried over $MgSO_4$. Removal of the solvent followed by trituration with methanol gave **3** as a white solid in 45% yield (1.29 g). ^{1}H NMR ($CDCl_3$, 400 MHz): δ 1.36 (s, 12H), 4.00 (s, 3H), 8.05 (d, J = 7.6 Hz, 1H), 8.10 (d, J = 7.6 Hz, 1H), 8.22 (s, 1H).

*Synthesis of Methyl 2-Cyano-5-(4,4,5,5-tetramethyl-1,3,2-dioxaborolan-2-yl)benzoate (**4**).* A 100 mL flask with a magnetic stirring bar, a septum inlet, and a condenser was charged with $Pd(dba)_2$ (0.13 g, 0.23 mmol) and tricyclohexylphosphine (0.15 g, 0.55 mmol) under nitrogen. Dioxane (27 mL) was added, and the resulting mixture was then stirred for 30 min at room temperature. Bis(pinacolato)diboron (2.11 g, 8.31 mmol), KOAc (1.12 g, 11.2 mmol), and **2** (1.50 g, 7.67 mmol) were added successively. After being stirred at 80 °C for 20 h, the reaction mixture was treated with water (30 mL). The product was extracted with toluene, washed with brine, and dried over $MgSO_4$. Removal of the solvent followed by trituration with methanol gave **4** as a white solid in 8.2% yield (181 mg). ^{1}H NMR ($CDCl_3$, 400 MHz): δ 1.36 (s, 12H), 4.00 (s, 3H), 7.79 (dd, J = 7.6, 0.6 Hz, 1H), 8.04 (dd, J = 7.6, 1.2 Hz, 1H), 8.22 (dd, J = 1.2, 0.6 Hz, 1H).

*Synthesis of Methyl 2-Cyano-4-((trimethyl-silyl)ethynyl)-benzoate (**5**).* A nitrogen-purged, stirred mixture of **1** (1.00 g, 5.11 mmol), a catalytic amount of CuI, $Pd(PPh_3)_4$ (0.60 g, 0.52 mmol), and ethynyltrimethylsilane (0.906 g, 9.22 mmol) in triethylamine (20 mL)/THF (24 mL) was heated to 75 °C for 16 h. After being cooled, the triethylamine hydrochloride was filtered, washed with additional CH_2Cl_2, and the combined filtrates evaporated under vacuum. The product was purified on a silica gel column with ethyl acetate/hexane (1/100, v/v) to obtain **5** in 31% yield (0.400 g). ^{1}H NMR ($CDCl_3$, 400 MHz): δ 0.27 (s, 9H), 4.00 (s, 3H), 7.70 (dd, J = 8.0, 1.6 Hz, 1H), 7.85 (d, J = 1.6 Hz, 1H), 8.08 (d, J = 8.0 Hz, 1H).

*Synthesis of 4-(7-(5-Bromothieno[3,2-b]thiophen-2-yl)-2,3-dihydrothieno[3,4-b][1,4]dioxin-5-yl)-N,N-bis(4-(hexyloxy)phenyl)aniline (**9**).* To a solution of **8** (0.543 g, 0.750 mmol) in DMF (7 mL) at 0 °C was added a solution of *N*-bromosuccinimide (0.134 g, 0.750 mmol) in DMF (5 mL). After 3 h of stirring at 0 °C, crushed ice was added, and the mixture was extracted with dichloromethane (3 × 12 mL). The combined organic layers were washed with water (3 × 60 mL) and dried over anhydrous $MgSO_4$. The solvent was removed with a rotary evaporator, and the residue was purified on a silica gel column with EtOAc/hexane (1/100, v/v) to obtain **9** in 60% yield (0.358 g). ^{1}H NMR (DMSO-d_6, 400 MHz): δ 0.88 (t, J = 7.2 Hz, 6H), 1.31 (m, 8H), 1.41 (m, 4H), 1.71 (m, 4H), 3.93 (t, J = 6.4 Hz, 4H), 4.37 (m, 2H), 4.42 (m, 2H), 6.78 (d, J = 8.8 Hz, 2H), 6.89 (d, J = 8.8 Hz, 4H), 7.01 (d, J = 8.8 Hz, 4H), 7.47 (d, J = 8.8 Hz, 2H), 7.51 (s, 1H), 7.61 (s, 1H). MS (ESI): m/z calcd for $C_{42}H_{42}BrNO_4S_3$, 803.16; found, 803.16 $[M^+]$.

*Synthesis of 4-((5-(7-(4-(Bis(4-(hexyloxy)phenyl)-amino)-phenyl)-2,3-dihydrothieno[3,4-b][1,4]dioxin-5-yl)thieno[3,2-b]thiophen-2-yl)ethynyl)-2-cyanobenzoic Acid (**KM-2**).* A 50 mL Schlenk flask containing bromide **9** (0.110 g, 0.137 mmol), **5** (0.0423 g, 0.164 mmol), piperidine (0.235, 2.74 mmol), $Pd(PPh_3)_4$ (0.023 g, 0.021 mmol), CuI (0.001 g, 0.0041 mmol), and K_2CO_3 (0.0426 g, 0.301 mmol) in THF (18 mL) and methanol (3 mL) was purged with N_2 for 5 min. The reaction mixture was refluxed for 48 h, and then H_2O (3 mL) was added. After the reaction was performed at 80 °C for 40 h, the mixture was diluted with H_2O and CH_2Cl_2, and then acidified with HCl under cooling. The organic layer was separated and subsequently dried over anhydrous $MgSO_4$. The solvent was removed with a rotary evaporator, and the residue was purified on a silica gel column with MeOH/CH_2Cl_2 (1/10, v/v) to obtain **KM-2** as a brown solid in 11% yield (14 mg). ^{1}H NMR (DMSO-d_6,400 MHz): δ 0.89 (t, J = 7.2 Hz, 6H), 1.31 (m, 8H), 1.42 (m, 4H), 1.71 (m, 4H), 3.94 (t, J = 6.4 Hz, 4H), 4.39 (m, 2H), 4.47 (m, 2H), 6.79 (d, J = 8.8 Hz, 2H), 6.90 (d, J = 8.8 Hz, 4H), 7.01 (d, J = 8.8 Hz, 4H), 7.49 (d, J = 8.8 Hz, 2H), 7.56 (s, 1H), 7.70 (s, 1H), 7.78 (dd, J = 8.4, 1.6 Hz, 1H), 7.92 (d, J = 1.6 Hz, 1H), 8.00 (d, J = 8.4 Hz, 1H). HR-MS (ESI): m/z calcd for $C_{52}H_{48}N_2O_6S_3$, 892.2675; found, 892.2676 $[M]^+$.

*Synthesis of 4-(5-(7-(4-(Bis(4-(hexyloxy)phenyl)amino)-phenyl)-2,3-dihydrothieno[3,4-b][1,4]dioxin-5-yl)thieno[3,2-b]thiophen-2-yl)benzoic Acid (**KM-3**).* The bromide **9** (0.0788 g, 0.0981 mmol), 4-(4,4,5,5-tetramethyl-1,3,2-dioxaborolan-2-yl) benzoic acid **6** (0.0292 g, 0.118 mmol), K_2CO_3 (0.059 g,

dx.doi.org/10.1021/jp304490a | J. Phys. Chem. C 2012, 116, 16876−16884

0.43 mmol), and $Pd(PPh_3)_4$ (0.012 g, 0.01 mmol) were dispersed in a mixture of THF (5 mL) and H_2O (1 mL). After the reaction was performed at 80 °C for 24 h, the mixture was diluted with H_2O and CH_2Cl_2, and then acidified with HCl under cooling. The organic layer was separated and subsequently dried over anhydrous $MgSO_4$. The solvent was removed with a rotary evaporator, and the residue was purified on a silica gel column with $MeOH/CH_2Cl_2$ (1/10, v/v) to obtain **KM-3** as brown solid in 17% yield (0.0144 g). ^1H NMR (DMSO-d_6, 400 MHz): δ 0.88 (t, J = 7.2 Hz, 6H), 1.31 (m, 8H), 1.41 (m, 4H), 1.70 (m, 4H), 3.93 (t, J = 6.4 Hz, 4H), 4.38 (m, 2H), 4.45 (m, 2H), 6.78 (d, J = 8.8 Hz, 2H), 6.89 (d, J = 8.8 Hz, 4H), 7.00 (d, J = 8.8 Hz, 4H), 7.49 (d, J = 8.8 Hz, 2H), 7.58 (s, 1H), 7.78 (d, J = 8.0 Hz, 2H), 7.98 (m, 3H). HR-MS (ESI): m/z calcd for $C_{49}H_{49}NO_6S_3$, 843.2722; found, 843.2747 $[M]^+$.

*Synthesis of 4-((5-(7-(4-(Bis(4-(hexyloxy)phenyl)-amino)-phenyl)-2,3-dihydrothieno[3,4-b][1,4]-dioxin-5-yl)thieno[3,2-b]thiophen-2-yl)ethynyl)benzoic Acid (**KM-5**).* A 50 mL Schlenk flask containing bromide **9** (0.110 g, 0.137 mmol), 4-((trimethylsilyl)ethynyl)-benzoic acid **7** (0.0897 g, 0.411 mmol), piperidine (0.235 g, 2.74 mmol), $Pd(PPh_3)_4$ (0.022 g, 0.019 mmol), CuI (0.001 g, 0.0041 mmol), and K_2CO_3 (0.0426 g, 0.301 mmol) in THF (15 mL) and methanol (3 mL) was purged with N_2 for 5 min. After the reaction was performed at 80 °C for 72 h, the mixture was diluted with H_2O and CH_2Cl_2, and then acidified with HCl under cooling. The organic layer was separated and subsequently dried over anhydrous $MgSO_4$. The solvent was removed with a rotary evaporator, and the residue was purified on a silica gel column with $MeOH/CH_2Cl_2$ (1/10, v/v) to obtain **KM-5** as a brown solid in 17% yield (19.9 mg). ^1H NMR (DMSO-d_6, 400 MHz): δ 0.88 (t, J = 7.2 Hz, 6H), 1.32 (m, 8H), 1.42 (m, 4H), 1.70 (m, 4H), 3.94 (t, J = 6.4 Hz, 4H), 4.39 (m, 2H), 4.45 (m, 2H), 6.79 (d, J = 8.8 Hz, 2H), 6.91 (d, J = 8.8 Hz, 4H), 7.02 (d, J = 8.8 Hz, 4H), 7.50 (d, J = 8.8 Hz, 2H), 7.57 (s, 1H), 7.61 (m, 2H), 7.76 (s, 1H), 7.95 (m, 2H). HR-MS (ESI): m/z calcd for $C_{51}H_{49}NO_6S_3$, 867.2722; found, 867.2747 $[M]^+$.

*Synthesis of 5-(5-(7-(4-(Bis(4-(hexyloxy)-phenyl) amino)-phenyl)-2,3-dihydrothieno[3,4-b][1,4]dioxin-5-yl)thieno[3,2-b]thiophen-2-yl)-2-cyanobenzoic Acid (**KM-6**).* Bromide **9** (0.267 g, 0.333 mmol), benzoate **4** (0.150 g, 0.522 mmol), K_2CO_3 (0.200 g, 1.45 mmol), and $Pd(PPh_3)_4$ (0.048 g, 0.04 mmol) were dispersed in a mixture of THF (20 mL) and H_2O (4 mL). After the reaction was performed at 80 °C for 48 h, the mixture was diluted with H_2O and CH_2Cl_2, and then acidified with 1 M HCl under cooling. The organic layer was separated and subsequently dried over anhydrous $MgSO_4$. The solvent was removed with a rotary evaporator, and the residue was purified on a silica gel column with $MeOH/CH_2Cl_2$ (1/10, v/v) to obtain **KM-6** as a brown solid in 21% yield (0.0615 g). ^1H NMR (DMSO-d_6, 400 MHz): δ 0.88 (t, J = 7.2 Hz, 6H), 1.30 (m, 8H), 1.40 (m, 4H), 1.69 (m, 4H), 3.92 (t, J = 6.4 Hz, 4H), 4.36 (m, 2H), 4.43 (m, 2H), 6.78 (d, J = 9.2 Hz, 2H), 6.89 (d, J = 8.8 Hz, 4H), 7.00 (d, J = 8.8 Hz, 4H), 7.47 (d, J = 8.8 Hz, 2H), 7.54 (s, 1H), 7.74 (d, J = 8.0 Hz, 1H), 7.80 (d, J = 8.0 Hz, 1H), 7.90 (s, 1H), 8.22 (s, 1H). HR-MS (ESI): m/z calcd for $C_{50}H_{48}N_2O_6S_3$, 868.2675; found, 868.2681$[M]^+$.

2.4. Differential Pulse Voltammetry (DPV) Measurements. The DPV of dyes was measured in DMF solution containing tetrabutylammonium hexafluoro-phosphate (0.1M) as a supporting electrolyte with glassy carbon as the working electrode and Pt as the counter electrode under Ar atmosphere. The redox potentials were calibrated with ferrocene as the internal reference.

2.5. Cell Fabrication. State-of-the art double layer mesoporous TiO_2 layer (6.6 μm of 20 nm particle (DSL 18NR-T, DYESOL) plus 6.7 μm of 400 nm light scattering particles (HPW-400NRD, CCIC)) was employed on FTO conducting glass (Solar-4 mm, Nippon Sheet Glass Co, Ltd.). The double layer TiO_2 film was sensitized by immersing it into a chloroform solution of the respective KM dye (0.1 mM) for 17 h at room temperature. The composition of the electrolyte was 1.0 M 1,3-dimethylimidazolium iodide, 30 mM I_2, 0.5 M *tert*-butylpyridine, and 0.1 M guanidinium thiocyanate in a mixture of acetonitrile and valeronitrile (85/15, v/v). A platinized FTO conducting glass (LOF TECH 7, Pilkington) was used as counter electrode. The spectral distribution of the light source simulates the AM 1.5G solar irradiation characteristics (Xe 450W/K113 (filter) with a spectral mismatch of less than 4%. The exposed area of the devices was 0.16 cm^2, a black tape mask being used to exclude any stray light. An antireflection film (ARCTOP, Mihama Co.) was attached on the photoanode side.

2.6. Photophysical Studies. Time-resolved transient absorption measurements were performed on dye-sensitized, 3 μm-thick, transparent TiO_2 mesoporous films screen-printed on nonconducting microscope slides immersed in dye-solutions. The pump−probe technique uses a compact CPA-2001, 1 kHz, Ti:Sapphire-amplified femtosecond laser (Clark-MXR), with a pulse width of about 120 fs and a pulse energy of 1 mJ at a central wavelength of 775 nm. The output beam was split into two parts for pumping a double-stage noncollinear optical parametric amplifier (NOPA) and to produce a white light continuum in a sapphire plate or 387 nm UV light by second harmonic generation of the CPA output in a thin BBO crystal. The NOPA was pumped by 200 μJ pulses at a central wavelength of 775 nm, and the excitation wavelength was tuned to 480 nm to generate pulses of approximately 10 μJ. The output pulses of the NOPA were compressed in a SF10-glass prism pair compressor down to a duration of less than 60 fs (fwhm). Iris diaphragms were used to decrease the pulse energy down to a few microjoules for the pump and to less than 1 μJ for the probe beam. Transient spectra were measured using a white light continuum (WLC) for probing.

The nanosecond laser flash photolysis employed 7 ns pulses to excite the sample at λ = 480 nm and using a 30 Hz repetition rate. A Powerlite 7030 frequency-doubled Q-switched Nd:YAG laser (Continuum, Santa Clara, CA) served as a light source. The laser beam output was expanded by a planoconcave lens to irradiate a large cross-section of the sample, whose surface was kept at a 30° angle to the excitation beam. The laser fluence on the sample was kept at a low level (40 μJ cm^{-2} per pulse) to ensure that, on average, less than one electron is injected per nanocrystalline TiO_2 particle on pulsed irradiation. The probe light, produced by a continuous wave xenon arc lamp, was first passed through a monochromator tuned at 650 nm, various optical elements, the sample, and then through a second monochromator, before being detected by a fast photomultiplier tube (Hamamatsu, R9110).

3. RESULTS AND DISCUSSION

3.1. Design and Synthesis of Sensitizers. Herein, we employed bis(*p*-hexyloxyphenyl)-aminophenyl as a donor, thienothiophene and a 3,4-ethylenedioxy-thiophene (EDOT) as a binary π-conjugated spacer, and various derivatives of

dx.doi.org/10.1021/jp304490a | J. Phys. Chem. C 2012, 116, 16876−16884

benzoic acids as electron acceptor/anchoring moieties for the D−π−A sensitizers as shown in Scheme 1. The strong electron-

Scheme 1. Synthesis of KM Dyes

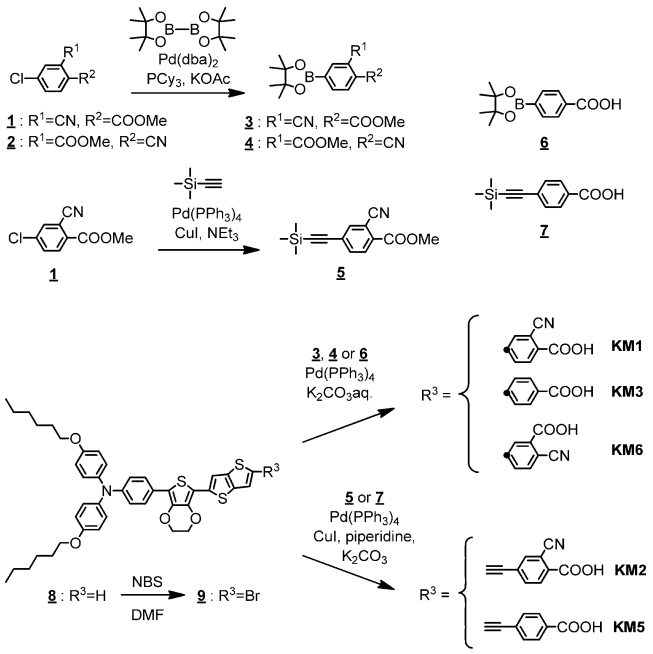

withdrawing nature of the cyano group substitution on the benzoic acid was expected not only to have an impact on the intramolecular charge transfer (ICT) transitions but also on the adsorption onto the TiO_2 surface.

Brief synthetic routes for the KM dyes are shown in Scheme 1. The coupling reagents **3**−**5** were prepared as new acceptor/anchoring parts. The important intermediate **8** was synthesized as previously reported.[5] Treatment of **8** with *N*-bromosuccinimide (NBS) gave the bromide **9**. The obtained **9** reacted with **3**, **4**, or **6** under the Suzuki coupling conditions to afford **KM-1**, **KM-6**, or **KM-3**, respectively. Sonogashira coupling reaction of **9** with **5** or **7** gave **KM-2** or **KM-5**, respectively.

3.2. Optical Properties. In the molecular structures of the sensitizers **KM-1**, **-2**, **-3**, **-5**, and **-6**, we have systematically varied the substitution of the −CN, −COOH, or acetylene bonds and studied their electronic properties. The UV−vis absorption spectra of all dyes in *N*,*N*′-dimethylformamide solutions are shown in Figure 1. The lowest energy peak position and molar absorption coefficients are tabulated in

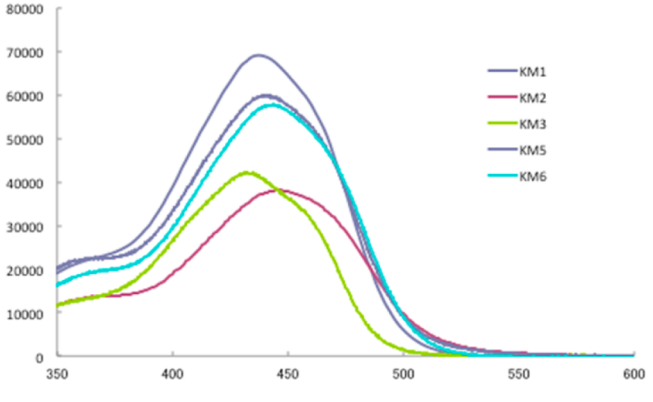

Figure 1. Absorption spectra of KM dyes in DMF.

Table 1. All dyes absorb strongly in the region between 320 and 550 nm with a broad maximum between 430 and 520 nm. The molar extinction coefficients of the peaks vary between 37 760 cm^{-1} M^{-1} for **KM-3** and 66 700 cm^{-1} M^{-1} for **KM-1**. Notably, the absorption of **KM-2** has a 13 nm red shift as compared to **KM-1**. Thus, it is safe to assume that the insertion of an acetylene linker between the thienothiophene unit and the cyano benzoic acid anchoring group slightly increases the π-conjugation. This observation is in line with the fact that the acetylene unit promotes a planar geometry as shown in the theoretical part. The absorption spectrum of **KM-2** dye is 6 nm red-shifted as compared to **KM-5** dye due to the insertion of the −CN group on the anchoring moiety. Dye **KM-3**, on the other hand, exhibits a significant blue shift in the absorption spectra as compared to the other dyes. This blue shift is due to the lack of the cyano group, which in **KM-1**, **KM-2**, and **KM-6** contributes to the enhancement of the π-system through resonance effects. In **KM-5**, the blue shift is compensated due to the acetylene unit, which shifts the absorption edge further to the red as compared to **KM-3** but not as far as compared to the cyano group containing dyes. From a comparison of the absorption features between **KM-2** and **KM-5** and between **KM-1**, **KM-2**, and **KM-6**, it can be seen that the cyano group rather than the acetylene unit has the main impact on the red-shift of the absorption edge. Fluorescence studies reveal comparable emission maxima at 620 nm for all of the dyes. Further, it is worth mentioning that the position of the cyano substituent on the benzoic acid also contributes to the shift of the spectral properties of the KM dyes.

3.3. Theoretical Investigation. To afford deeper insight into the geometrical and electronic properties of the dyes, the geometries of the neutral and oxidized forms of the molecules were optimized using density functional theory (DFT) with the B3LYP[6]/6-31G(d)[7] method as implemented in the Gaussian 09[8] program package. The structures of the neutral molecules are depicted in Figure S1. No significant geometrical changes were found upon oxidation of the molecules. Notably, in all dyes the aromatic rings of the bridge between triphenylamine (TPA) and the anchoring groups do not deviate from planarity and comprise dihedral angles of less than 5° except for the last phenyl ring of the benzoic acid. In **KM-1**, **KM-3**, and **KM-6**, this phenyl ring is twisted by 20° with respect to the thienothiophene group. In **KM-2** and **KM-5**, on the other hand, it is entirely in plane with the thienothiophene due to the acetylene linker, which increases the distance between the phenyl p-orbitals and the sulfur d-orbitals. An increased distance allows for a conformation in which the steric hindrance due to the *ortho*-hydrogen electrostatic repulsion is minimized. This strongly favors an entirely planar configuration, simultaneously maximizing the π-conjugation pathway.

Insight into the dependence of the electronic properties on the molecular structure, particularly with respect to the anchoring groups and the variations of the linker between them and TPA, was provided by the analysis of the frontier orbitals (Figure 2). The highest occupied orbitals (HOMOs) and the lowest unoccupied orbitals (LUMOs) perfectly reveal the donor−acceptor character of the TPA and the anchoring groups, respectively. Such dye architecture provides an energy gradient for the excitation and facilitates the HOMO to LUMO charge transfer transition, which is crucial to afford a favorable energetic pathway for electron injection into the TiO_2 surface. As seen in Figure 2, the HOMO, which is localized on the TPA unit, conjugates deeply into the bridge and provides good

dx.doi.org/10.1021/jp304490a | J. Phys. Chem. C 2012, 116, 16876−16884

Table 1. Optical and Electrochemical Properties of Dyes[a]

dye	λ_{max} (nm)	$\sum$ (M^{-1} cm^{-1})	HOMO (eV)	LUMO (eV)	HOMO (DFT)	LUMO (DFT)	E_{ox1} (V)	E_{ox2} (V)	E_{red1} (V)	E_{red2} (V)
KM-1	437	66 700	−5.41	−3.10	−4.56	−2.29	0.19	0.46	−2.14	−2.63
KM-2	445	38 070	−5.44	−2.94	−4.57	−2.41	0.22	0.46	−2.28	−2.63
KM-3	432	37 760	−5.42	−2.77	−4.45	−1.89	0.20	0.42	−2.45	−2.73
KM-5	439	60 000	−5.48	−2.92	−4.48	−2.05	0.26	0.44	−2.30	−2.50
KM-6	443	57 820	−5.42	−2.94	−4.55	−2.24	0.20	0.45	−2.28	−2.49

[a]All potential values are in V vs Fc/Fc^+. Dyes were dissolved in DMF. Redox potential of Fc/Fc^+ in DMF is 0.720 V vs NHE. HOMO and LUMO energy levels of KM dyes were experimentally determined from the first oxidation and reduction potentials, measured using differential pulse voltammetry.

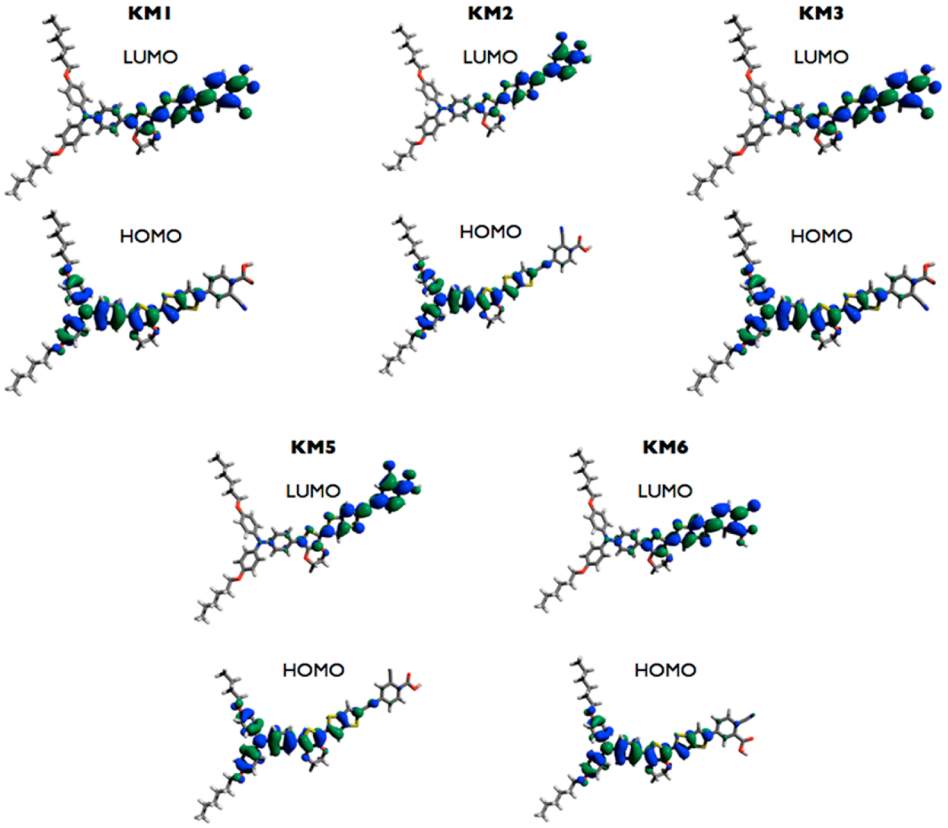

Figure 2. Frontier orbital schemes of the neutral species of the dyes as computed by DFT (B3LYP/6-31G(d)).

overlap with the LUMO, which has the greatest coefficients on the anchoring part of the dye. This rationalizes good electronic communication through the linker between both moieties. A closer look at the HOMO coefficients reveals the impact of the subtle variations of molecular structure in these systems. First, let us consider the influence of the acetylene linker on the overall conjugation. Remarkably, in both **KM-2** and **KM-5**, the acetylene bond provides a reasonable conjugation into the anchoring groups. This is due to the preservation of the perfect planarity as mentioned above. Orbital coefficients of the HOMO can be found up to the oxygen atoms of the anchoring groups. In the presence of the cyano group with its electron-withdrawing effect, the coefficients on the oxygen atoms are somewhat smaller. In the remaining dyes, these coefficients are slightly greater, which is due to the shorter length of the linker. However, the differences relatively to **KM-2** and **KM-5** are only subtle. Because of the 20° twist of the last phenyl ring, the π-conjugated pathway is distorted in **KM-1**, **KM-3**, and **KM-6**. Interestingly, it seems that the *para*-position of the cyano group as present in **KM-6** provides the longest conjugated pathway.

To summarize, the insertion of the acetylene bond does not alter the extent of the π-conjugation. The unfavorable augmentation in bond-length alteration is compensated by the propagation of planarity, which actually enhances the conjugation as seen from absorption studies. In **KM-1**, **KM-3**, and **KM-6**, on the other hand, the lack of the acetylene bond induces 20° torsion to minimize electrostatic repulsion. Hence, one may say that in all dyes the binding to TiO_2 guarantees comparable prerequisites for charge injection. Examining the anchoring groups from an electronic point of view, one may clearly say that introducing a cyano group into the *para*-position, as it is the case in **KM-6**, provides the best π-conjugation throughout the whole molecule. Furthermore, it is important to keep in mind that the variation of the anchoring groups will also alter the binding modes to TiO_2 and, thus, parameters such as dye loading or the surface orientation of the dyes.

Considering the LUMO orbitals of the oxidized species (Figure S2), the distribution of electron density nicely corroborates the preservation of the π-system upon oxidation

because they resemble the HOMO orbitals of the neutral species. In other words, a clean HOMO to LUMO charge transfer is expected upon oxidation, and the HOMO becomes the LUMO in the oxidized form of the dyes. Notably, oxidation highly increases the electron density on the cyano group in **KM-6**, which is expected to accelerate charge injection into the TiO_2 film.

The calculated HOMO−LUMO energies follow the trends as found by electrochemical analysis and are listed in Table 1 for comparison. A closer look at the energies reveals their dependence on the anchoring groups. Dyes comprising the cyano group have significantly lower HOMO−LUMO gaps. This is basically due to the fact that the cyano group exerts an electron-withdrawing effect and induces a charge shift of the HOMO, which favors the delocalization of π-orbitals across the bridge and therefore lowers the energies of the HOMOs on average by 0.1 eV. An even stronger impact of the cyano group is found considering the LUMO energies. These are on average more than 0.2 eV lower in **KM-1**, **KM-2**, and **KM-6** due to the enhancement of the π-system through resonance effects with the carboxylic functional group.

3.4. Electrochemical Properties. As shown above, the position and the nature of the substituents have an influence on the electronic properties of the KM dyes. Thus, we have employed differential pulse voltammetry measurements to examine the effects on the redox properties. The redox potentials as obtained in DMF solutions are listed in Table 1 and shown in Figure S3. Notably, we encountered an error in the previously reported redox potential of **KM-1** dye and corrected the value to 0.19 V instead of 0.39 V.[5] A comparison of the potentials of **KM-1**, **KM-3**, and **KM-6** shows that the −CN group and its position on the benzoic acid anchor have negligible effects. On the other hand, inserting an acetylene bond between thienothiophene and the anchoring group (**KM-2** and **KM-5**) leads to an increase of the redox potentials by 30 and 60 mV as compared to **KM-1** and **KM-3**, respectively. As expected from the theoretical investigation, the substitution patterns mainly govern the differences in the LUMO levels. Comparing the reduction potential **KM-1** and **KM-3** indicates that introducing cyano group in the benzoic acid lowers the reduction potential by 310 mV due to electron-withdrawing nature. This effect is reduced when comparing the reduction potential of **KM-2** and **KM-5** dyes where an acetylene linker is used as a spacer.

3.5. Photovoltaic Properties. Figure 3 shows the incident photon-to-current conversion efficiency (IPCE) action spectra of the DSCs with **KM-1**, **-2**, **-3**, **-5**, **-6** dyes. The corresponding photocurrent−voltage curves are shown in Figure 4, and the photovoltaic parameters are summarized in Table 2. As seen from Figure 3, **KM-6** exhibits the widest spectral response among the five investigated dyes. The maximum IPCE value for **KM-6** reached 80% at 480 nm, exceeding 70% from the 430−530 nm range with a tail extending up to 650 nm. On the other hand, **KM-5** reveals its highest IPCE with a value of 65% at 470 nm and a tail reaching only 600 nm. In general, the IPCE spectral response of **KM-1**, **KM-2**, **KM-3**, and **KM-5** is lower than that of **KM-6**, which is also reflected by the lower J_{sc} values and PCEs. Furthermore, it is interesting to see that the −CN group substituted at the *para*-position shifts the spectral response more to the red than in the corresponding *meta*-position. From a comparison of the J_{sc} values (Table 2) of all assembled devices, it is seen that the **KM-6** device manifests the highest J_{sc} with a value of 8.05 mA cm^{-2} under full sunlight

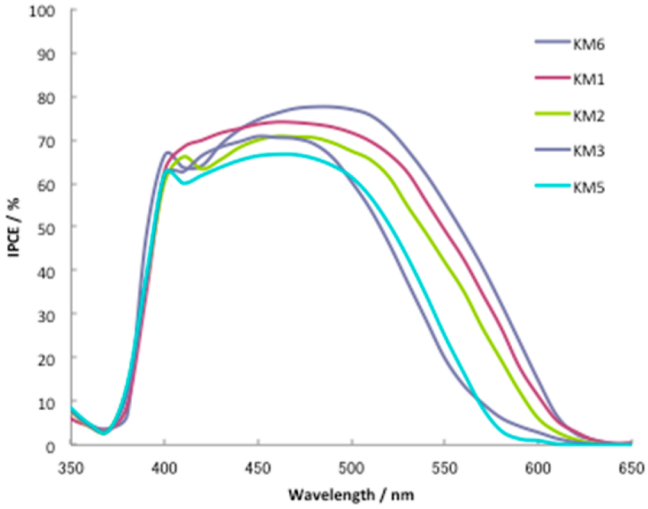

Figure 3. Incident photon-to-current conversion efficiency spectra of DSC devices with KM dyes.

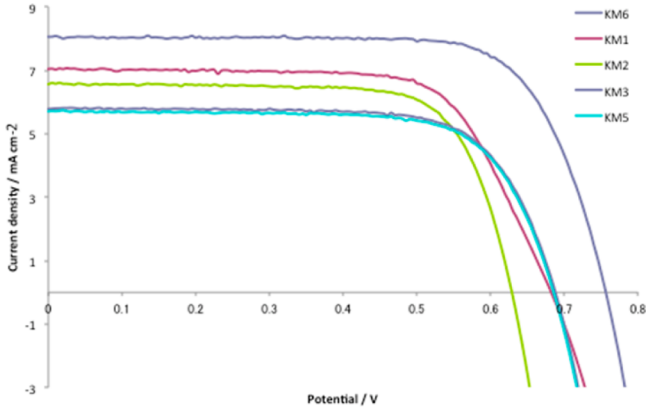

Figure 4. J-V curves of DSC devices sensitized with KM dyes under full sun simulated AM 1.5G (100mW/cm^2) illumination.

Table 2. Photovoltaic Parameters of KM-1, 2, 3, 5, 6-Sensitized Solar Cells under Illumination of AM 1.5G (100 mW cm^{-2}) Simulated Solar Light

dye	J_{sc} (mA cm^2)	V_{oc} (V)	FF	PCE (%)
KM-1	7.04	0.682	0.691	3.32
KM-2	6.56	0.629	0.737	3.02
KM-3	5.78	0.688	0.718	2.87
KM-5	5.70	0.685	0.717	2.82
KM-6	8.05	0.756	0.733	4.50

intensity. The J_{sc}'s of the **KM-1**, **KM-2**, and **KM-6** devices are higher than that of **KM-3** due to their broader spectral response as seen from their IPCE characteristics. Finally, **KM-6** exhibits the highest V_{oc} reaching 0.756 V among of the five **KM** dyes.

Overall, the obtained power conversion efficiencies (PCEs) range from 3.32% to 4.50% for the **KM-1** and **KM-6** device, respectively. Upon the introduction of the cyano substituents on the acceptor units, the corresponding PCEs turn out to be higher than those of the dyes lacking a cyano substituent. Hence, it is reasonable to state that introducing a cyano substituent on the benzene acceptor/anchoring moiety leads to an improvement of the DSC performance. Two effects are responsible for this trend as shown in the theoretical part. First, the cyano moiety improves the ICT nature, and, second, it

dx.doi.org/10.1021/jp304490a | J. Phys. Chem. C 2012, 116, 16876−16884

allows for a better adsorption on TiO_2. Moreover, the dyes with the cyano substituent in *para*-position showed a better photovoltaic performance in contrast to the *meta*-position (see **KM-1** and **KM-6**). With the **KM-3** and **KM-5** devices, we obtained PCE values of 2.87% and 2.82%, respectively. Inserting an acetylene bond between the thienothiophene spacer and the benzoic acid showed no significant influence on the photovoltaic performance of **KM-3**. However, **KM-2**, which has both an acetylene bond and a cyano substituent, exhibits a higher PCE than **KM-3**. This is due to the higher J_{sc} value, although the V_{oc} is lower.

3.6. Photophysical Properties. Various spectroscopic investigation methods were employed to shed light onto the differences in the photovoltaic performance of the dyes. Photoinduced absorbance spectroscopic studies were employed to disclose the absorbance changes upon photoexcitation. All dyes adsorbed on the surface of TiO_2 revealed similar features, that is, a singlet bleaching in the region between 400 and 600 nm and two absorption maxima, one at 680 nm and another extending from 900 to 1600 nm as shown for **KM-3** (Figure S4). Because of the donor–bridge–acceptor type of chemical architecture, a charge transfer occurs between the triphenylamine (TPA) donor and the electron-accepting anchoring groups. Hence, the ground-state bleaching is assigned to the charge transfer excitation between the TPA through the π-conjugated bridge to the anchoring group, whereas the other two maxima correspond to the radical cation of the TPA–$TPA^{\bullet+}$.[9]

Complementary time-resolved transient absorption measurements were performed to scrutinize the dynamics of charge separation and charge recombination of the dyes adsorbed on TiO_2. Thereby, we focused exclusively on the generation of the TPA radical cation. To resolve the fast charge separation processes, the transient absorption spectral changes were investigated on the femtosecond time scale. 480 nm light source was chosen to excite the ground state, which instantaneously results in a ground-state bleaching between 480 and 540 nm. After only 0.5 ps, the bleaching shifts to the red by 20 nm and is accompanied by the formation of absorption with a broad maximum between 580 and 750 nm. The latter is attributed to the radical cation signal of the TPA. Hence, the photoexcitation of the chromophoric units results in a rapid electron transfer from the dye to TiO_2 and the formation of a charge separated state. After formation, the TPA radical cation signal and the ground-state bleaching are persistent on the time-scale of our femtosecond experiments. This proves that upon irradiation an instantaneous transduction of singlet-excited state energy powers the charge separation process. The transient absorption spectra of all KM dyes exhibit similar features, and a representative example is shown in Figure 5, top.

The formation of the radical ion pairs occurs with different rate constants for the various dyes. After 3 ps, for instance, the $TPA^{\bullet+}$ signatures are already fully developed in **KM-1**, **KM-2**, and **KM-6**, whereas their formation in **KM-3** and **KM-5** requires more than 15 ps. A comparison of the rate constants as obtained by monoexponential fitting of the time–absorption profiles (Figure 5, bottom) of the above-mentioned features is presented in Table 3. Remarkably, the most significant influence on the rates is imposed not by the distance between the donor and the acceptor unit but by the anchoring groups. A likely rationale is that, due to the improved binding modality of the cyanobenzoic acid groups[5] with regard to the benzoic acid

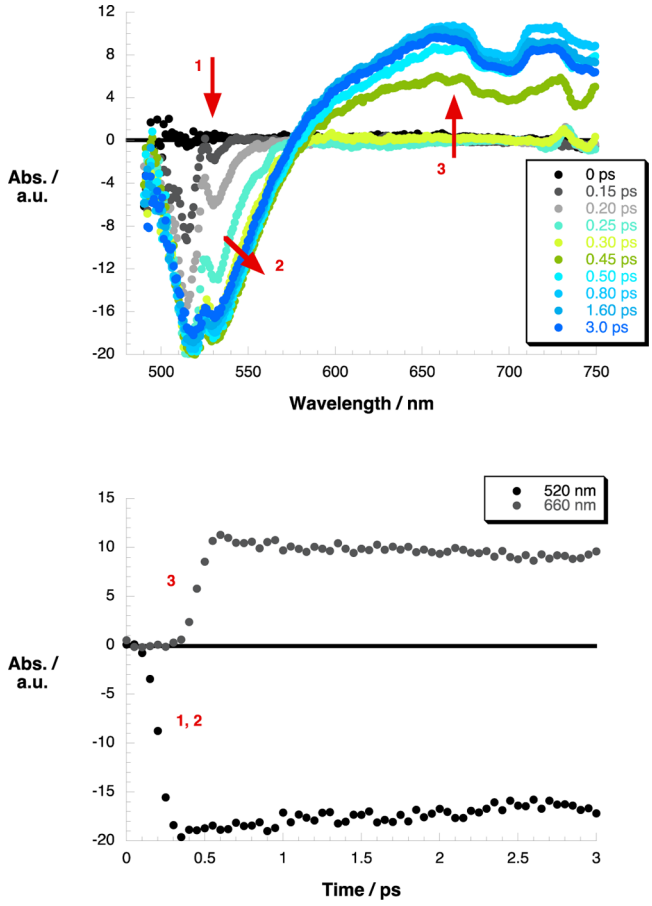

Figure 5. Top: Differential absorption spectrum obtained upon femtosecond flash photolysis (λ_{exc} = 480 nm) of a film of **KM-2** on 3 μm thick TiO_2 with several time delays between 0 and 3 ps at room temperature, illustrating (1) the transformation of the ground-state transient bleaching signal between 480 and 540 nm, (2) the $TPA^{\bullet+}$ radical cation signature represented by the shift of the bleaching, and (3) the development of a new positive band beyond 560 nm. Bottom: Time–absorption profiles illustrating the dynamics for the singlet-state bleaching (520 nm) and the radical cation formation (660 nm). The numbers correspond to the signals mentioned above.

Table 3. Charge Separation (CS) and Recombination (CR) Rates and the Corresponding Lifetimes of the Dyes

	k_{CS}/s^{-1}	τ_{CS}/ps	k_{CR}/s^{-1}	$\tau_{CR}/\mu s$
KM-1	4.00×10^{11}	2.4	5.36×10^{3}	186.7
KM-2	4.15×10^{11}	2.4	2.52×10^{3}	397.5
KM-3	6.62×10^{10}	15.1	3.00×10^{3}	333.3
KM-5	3.69×10^{10}	27.1	2.49×10^{3}	401.7
KM-6	3.23×10^{11}	3.1	1.09×10^{3}	921.2

groups, the charge injection into TiO_2 is facilitated in **KM-1**, **KM-2**, and **KM-6**. Considering the spacer between the bridge and the anchor, the triple bond (in **KM-2** and **KM-5**) provides very efficient electronic communication (see theoretical section). Hence, inserting the acetylene groups does not significantly affect the π-conjugation pathway and therefore leaves the charge separation rate constants nearly unchanged. This is seen from the comparison of the lifetimes for **KM-1** with **KM-2** and **KM-3** with **KM-5**.

Taking into account that the dyes exhibit a donor–π-bridge–acceptor architecture, we assumed the charge transfer rates to be dependent on the distance between donor and acceptor with

dx.doi.org/10.1021/jp304490a | J. Phys. Chem. C 2012, 116, 16876–16884

the electrons being transferred through the π-bridge. Such a through-bridge charge transfer leads to a molecular-wire behavior of the moieties linking TPA to the anchoring groups. Hence, plotting the charge separation rates as a function of the distance between TPA and the anchoring groups allowed for the determination of the attenuation factor β of the dyes. The slopes of the linear fits of the charge separation rates afforded a very low β value of 0.04 $Å^{-1}$ (Figure S5). Therefore, the dependence of the charge separation rates on the length of the electron transfer distance turned out to be weak, indicating efficient conjugation between the donor and acceptor moieties.

Interestingly, identical rates are obtained by fitting the signals of both the singlet-excited state and the charge-separated state. This hints to the fact that an extremely fast and instantaneous transduction of singlet-excited state energy powers the charge separation processes. This is in line with the fact that efficient conjugation provides good electronic communication between the building blocks, that is, donor, π-bridge, and acceptor.

To obtain information about the decay dynamics of the oxidized state of the dyes, we moved to corresponding nanosecond laser flash photolysis experiments performed on TiO_2 films in the absence and presence of a redox electrolyte. The recorded spectra (Figure 6) corroborated the results obtained throughout the photoinduced absorbance studies and

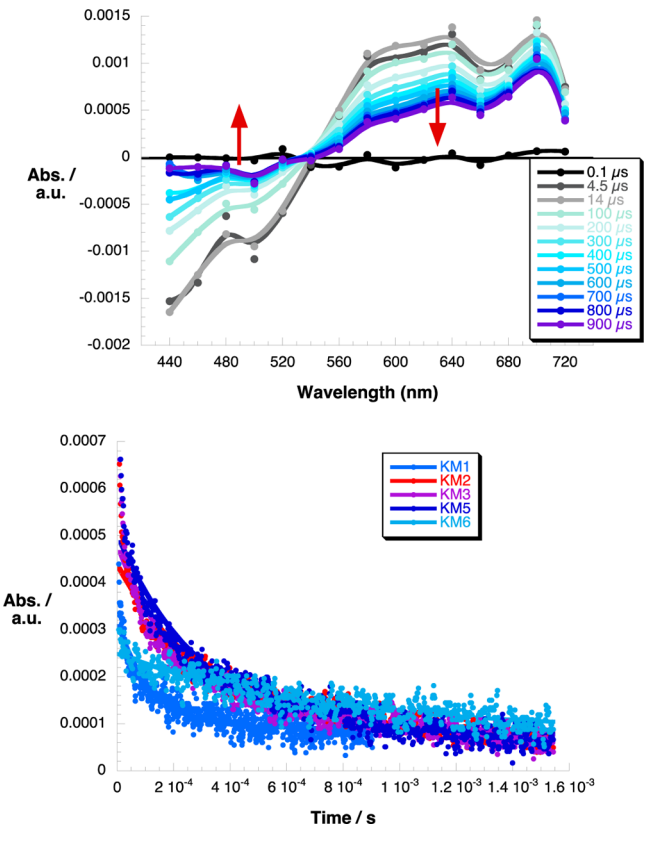

Figure 6. Top: Differential absorption spectrum obtained upon nanosecond flash photolysis of a thin film of **KM-3** on 3 μm thick TiO_2 in the absence of redox electrolyte with several time delays between 0 and 0.9 ms at room temperature, illustrating the decay of the signal of the radical cation with the ground-state transient bleaching between 400 and 540 nm and the $TPA^{\bullet+}$ signature from 560 to 720 nm. Bottom: Time−absorption profiles illustrating the dynamics of the decay of the radical cation signals of all dyes at 760 nm.

the femtosecond transient absorption measurements. Upon 480 nm excitation, all dyes show the presence of a singlet bleaching between 420 and 520 nm and a broad absorption band between 560 and 720 nm. In line with the photoinduced absorbance studies, the decay dynamics in the NIR region between 760 and 1100 nm were probed as well. In general, the dynamics of the charge recombination occur on a time-scale of hundreds of microseconds. **KM-2**, **KM-3**, and **KM-5** show comparable dynamics. The charge recombination in **KM-2** and **KM-5** is slightly longer by approximately 100 μs, which may be attributed to the extended distance due to the triple bond. More interestingly, changing the cyano anchor from the *meta*- to *para*-position increases the charge recombination lifetime by a factor of 5 from 186 μs in **KM-1** to 921 μs in **KM-6** (see Table 3). Further, the remarkably long charge recombination in **KM-6** provides an explanation for the outstanding IPCE values of the **KM-6** cells as compared to the remaining dyes.

Concluding, both the distance between the TPA donors and the anchoring groups and the anchoring groups themselves govern the charge recombination lifetimes. On one hand, increasing the separation distance decelerates the back transfer process of the dye-injected electrons from TiO_2 to the oxidized donor. On the other, little structural variations of the anchor, as present in **KM-1** and **KM-6**, may already change the binding modes to the surface and therefore vary the electronic coupling between the oxidized TPA donor and the TiO_2 surface. This, in turn, influences the back-electron transfer. Possibly, a chelating effect dependent on the position of the cyano-carboxylic anchor also leads to faster charge recombination due to a minimization of trapping states on the TiO_2 surface.

Obviously, exchanging the positions of the cyano and carboxylic groups in **KM-6** changes the adsorption geometry. In particular, it will lead to a higher tilt angle of the adsorbed molecule as compared to **KM-1**. A higher tilt angle, on the other hand, destabilizes the binding to TiO_2 and increases the intermolecular interactions between individual molecules, which implies better stabilization of the oxidized state within the interacting π-systems of the molecules on the surface.[10] Consequently, a slower back-electron transfer to the oxidized dye molecule and longer lifetimes of the oxidized states are observed. Furthermore, slight changes of the binding geometry may already have a significant impact on the charge transfer rates due to possible through-space interactions.[11] It should also be taken into account that with the exchange of the carboxylic acid group from the *para*- to the *meta*-position, not only the π-conjugation length changes but also the electronic coupling into TiO_2,[5] which strongly affects the charge transfer. However, to gain full understanding of the impact of such structural changes, the orientation of the molecules on the surface should be analyzed by means of surface-sensitive techniques such as XPS or NEXAFS.

Considering **KM-2** and **KM-5**, the slightly larger separation distance between donor and anchoring group due to the inserted acetylene linker is responsible for their slightly slower recombination dynamics. The addition of the redox electrolyte solution accelerates the dye regeneration of the anchored dye species in all **KM** dyes, and this process is independent of dye structure.

Plotting the charge recombination rates as a function of distance between the TPA and the anchoring groups allowed for the determination of the attenuation factor β also for charge recombination (Figure S6). Without considering **KM-6**, the slopes of the linear fits of the data points reflect a deceleration

dx.doi.org/10.1021/jp304490a | J. Phys. Chem. C 2012, 116, 16876−16884

of the charge recombination with increasing separation distance between the donor and the anchoring groups. The β value in the absence of electrolyte solution was found to be 0.18 $Å^{-1}$.

The increased value of β with regard to charge separation implies that the back electron transfer depends on the length of the linker more strongly than for charge separation. However, when considering the attenuation factor, the influence of the anchoring groups is not taken into account. Therefore, nevertheless, a high β value does not necessarily rule out efficient conjugation through the linkers. As shown in the theoretical investigation, the π-system is retained upon oxidation. The geometries of the oxidized form of the dyes preserve their planarity. All together, this clearly underlines the importance and role of the anchoring groups in the charge recombination.

In conclusion, the photophysical studies reveal that for both charge separation and charge recombination, the most significant parameter for governing the charge transfer turned out to be the anchoring to TiO_2. It was shown that the cyano substituents clearly enhance the electronic coupling between the dye and TiO_2. Together with the spectral response of the cell, the binding modes are assumed to control the photovoltaic performances of the DSCs based on the **KM** dyes.

4. CONCLUSIONS

In summary, we designed and synthesized five new organic sensitizers with cyano and/or triple bond substituted benzoic acid as an acceptor/anchoring group. As a result, the cyano substituent showed improved DSC performances. In contrast, introducing both a cyano substituent and a triple bond into this structure did not lead to a further improvement due to the larger distance between donor and acceptor/anchoring moieties of the dyes. Thus, the DSC device based on **KM-6**, composed of a *para*-cyano benzoic acid as an acceptor/anchoring group, revealed the best performance with a maximum IPCE of 80% and a PCE of 4.5% at AM 1.5 G illumination (100 mW cm^{-2}). Currently, we are investigating this novel acceptor/anchoring group linked to various π-conjugated spacers. We expect that improving the intramolecular transfer of electrons from HOMO to LUMO will lead to an enhanced device performance.

■ ASSOCIATED CONTENT

Ⓢ Supporting Information

Geometries of the computed structures, LUMO representations of the oxidized structures, photoinduced absorbance spectra, and rate constants versus donor−acceptor distance dependence. This material is available free of charge via the Internet at http://pubs.acs.org.

■ AUTHOR INFORMATION

Corresponding Author

*E-mail: shaik.zakeer@epfl.ch (S.M.Z.), michael.graetzel@epfl.ch (M.G.).

Notes

The authors declare no competing financial interest.

■ ACKNOWLEDGMENTS

We thank the Swiss National Science Foundation and EU SPI Cooperation, Collaborative project INNOVASOL, FP7-NMP3-SL-2009-227057, Grant agreement Number 22 for financial support. We are grateful to Dr. Tsuguo Koyanagi from JGC C&C (Japan), Dyesol (Australia), Nippon Sheet Glass Co., Ltd., and Mihama Co., for providing the 400 nm sized TiO_2 particles, the 20 nm particles (DSL 18NR-T), the FTO glass, and antireflection layer, respectively. We thank Dr. Carole Grätzel, Dr. Etienne Baranoff, and Dr. Yum Jun-Ho for fruitful discussions. M.K. is grateful to Kureha Corp. for scholarship support. M.W. and J.-E.M. thank NCCR MUST, a research instrument of the Swiss National Science Foundation, for generous support.

■ REFERENCES

(1) Grätzel, M. *Acc. Chem. Res.* **2009**, *42*, 1788−1798.

(2) (a) Chen, C.; Wang, M.; Li, J.; Pootrakulchote, N.; Alibabaei, L.; Ngoc-le, C.; Decoppet, J.; Tsai, J.; Grätzel, C.; Wu, C.; et al. *ACS Nano* **2009**, *3*, 3103−3109. (b) Gao, F.; Wang, Y.; Shi, D.; Zhang, J.; Wang, M.; Jing, X.; Humphry-Baker, R.; Wang, P.; Zakeeruddin, S. M.; Grätzel, M. *J. Am. Chem. Soc.* **2008**, *130*, 10720−10728. (c) Yu, Q.; Wang, Y.; Yi, Z.; Zu, N.; Zhang, J.; Zhang, M.; Wang, P. *ACS Nano* **2010**, *4*, 6032−6038. (d) Chiba, Y.; Islam, A.; Watanabe, Y.; Komiya, R.; Koide, N.; Han, L. *Jpn. J. Appl. Phys.* **2006**, *45*, L638−L640. (e) Yella, A.; Lee, H.-W.; Tsao, H. N.; Yi, C.; Chandiran, A. K.; Nazeeruddin, M. K.; Diau, E. W.-G.; Yeh, C.-Y.; Zakeeruddin, S. M.; Grätzel, M. *Science* **2011**, *334*, 629−634.

(3) (a) Zhang, G.; Bala, H.; Cheng, Y.; Shi, D.; Lv, X.; Yu, Q.; Wang, P. *Chem. Commun.* **2009**, 2198−2200. (b) Zeng, W.; Cao, Y.; Bai, Y.; Wang, Y.; Shi, Y.; Zhang, M.; Wang, F.; Pan, C.; Wang, P. *Chem. Mater.* **2010**, *22*, 1915−1925. (c) Ito, S.; Miura, H.; Uchida, S.; Takata, M.; Sumioka, K.; Liska, P.; Comte, P.; Pechy, P.; Grätzel, M. *Chem. Commun.* **2008**, 5194−5196. (d) Li, R.; Liu, J.; Cai, N.; Zhang, M.; Wang, P. *J. Phys. Chem. B* **2010**, *114*, 4461−4464. (e) Zhu, W.; Wu, Y.; Wang, S.; Li, W.; Li, X.; Chen, J.; Wang, Z.-S.; Tian, H. *Adv. Funct. Mater.* **2011**, *21*, 756−763. (f) Marszalek, M.; Nagane, S.; Ichake, M.; Humphry-Baker, R.; Paul, V.; Zakeeruddin, S. M.; Grätzel, M. *J. Mater. Chem.* **2012**, *22*, 889−894. (g) Qin, C.; Islam, A.; Han, L. *Dyes Pigm.* **2012**, *94*, 553−560.

(4) (a) Mishra, A.; Fischer, M.; Bäuerle, P. *Angew. Chem., Int. Ed.* **2009**, *48*, 2474−2499 and references cited therein. (b) Alibabaei, L.; Kim, J.-H.; Wang, M.; Pootrakulchote, N.; Teuscher, J.; Di Censo, D.; Humphry-Baker, R.; Moser, J.-E.; Yu, Y.-J.; Kay, K.-Y.; et al. *Energy Environ. Sci.* **2010**, *3*, 1757−1764. (c) Hagfeldt, A.; Boschloo, G.; Sun, L.; Kloo, L.; Pettersson, H. *Chem. Rev.* **2010**, *110*, 6595−663 and references cited therein.

(5) Katono, M.; Bessho, T.; Meng, S.; Humphry-Baker, R.; Rothenberger, G.; Zakeeruddin, S. M.; Kaxiras, E.; Grätzel, M. *Langmuir* **2011**, *27*, 14248−14252.

(6) Stephens, P. J.; Devlin, F. J.; Chablowski, C. F.; Frisch, M. *J. Phys. Chem.* **1994**, *98*, 11623−11627.

(7) Rassolov, V. A.; Pople, J. A.; Ratner, M. A.; Windus, T. L. *J. Chem. Phys.* **1998**, *109*, 1223−1229.

(8) Frisch, M. J.; et al. *Gaussian 09*; Gaussian, Inc.: Wallingford, CT, 2009.

(9) (a) Oyama, M.; Higuchi, T.; Okazaki, S. *Electrochem. Solid-State Lett.* **2002**, *5*, E1−E3. (b) Fantacci, S.; De Angelis, F.; Nazeeruddin, M. K.; Gratzel, M. *J. Phys. Chem. C* **2011**, *115*, 23126−23133. (c) Julio, R.; Pinzón, J. R.; Gasca, D. C.; Gayathri, S.; Bottari, G.; Torres, T.; Guldi, D. M.; Echegoyen, L. *J. Am. Chem. Soc.* **2009**, *131*, 7727−7734.

(10) (a) Schnadt, J.; Schiessling, J.; O'Shea, J. N.; Gray, S. M.; Patthey, L.; Johansson, M. K. J.; Shi, M.; Krempasky, J.; Ahlund, J.; Karlsson, P. G.; Persson, P.; Martensson, N.; Bruhwiler, P. A. *Surf. Sci.* **2003**, *540*, 39−54. (b) Thomas, A. G.; Syres, K. L. *Chem. Soc. Rev.* **2012**, *41*, 4207−4217 and references therein.

(11) Imahori, H.; Kang, S.; Hayashi, H.; Haruta, M.; Kurata, H.; Isoda, S.; Canton, S. E.; Infahsaeng, Y.; Kathiravan; Pascher, A. T.; et al. *J. Phys. Chem. A* **2011**, *115*, 3679−3690.